Taylor & Francis
Taylor & Francis Group

Investigating low-frequency dielectric properties of a composite using the distribution of relaxation times technique

ENIS TUNCER*†, NICOLA BOWLER‡, I. J. YOUNGS§ and
K. P. LYMER¶

†High Voltage and Dielectrics, Applied Superconductivity Group
Fusion Energy Division, Oak Ridge National Laboratory
One Bethel Valley Road, Oak Ridge, TN 37831-6122 USA
‡Center for Nondestructive Evaluation, 279 Applied Sciences Complex II
1915 Scholl Road, Ames, Iowa 50011-3042 USA
§Physical Sciences Department, DSTL, Porton Down
Salisbury, Wiltshire, SP4 0JQ, UK
¶Future Systems Technology Division, QinetiQ Ltd
Farnborough, Hampshire, GU14 0LX, UK

The distribution of relaxation times approach, a less frequently employed dielectric data analysis technique, is utilized to better understand the relaxation characteristics of composites consisting of metal-coated, hollow glass spheres dispersed in a paraffin wax matrix. The dielectric properties of the composite samples are measured by means of impedance spectroscopy in the frequency range 0.1 mHz to 10 MHz. The application of a mixture law is not appropriate for the analysis of the frequency-dependent properties of the considered system on this broad frequency range. However, utilization of the distribution of relaxation times procedure to study the dielectric behaviour shows clear trends in the mixtures' relaxation spectra. Relaxation processes of the paraffin wax and those specific to the composites are found from the extracted distribution of relaxation times spectra. The influence of the filler concentration, q, on the dielectric properties is examined; a relaxation with a narrow distribution at intermediate frequencies becomes broad with the addition of the filler. This relaxation, in the form of the low-frequency-dispersions (also known as constant phase angle) phenomenon, dominates the dielectric properties of the composites with high bead concentration, $q > 0.15$. The variation in dielectric properties of individual samples whose bead concentrations q are nominally the same is discussed in terms of possible microstructural variations.

1. Introduction

Dielectric properties of materials have attracted both theoreticians and experimentalists for more than a century. A comprehensive knowledge of the

---

*Corresponding author. Email: enis.tuncer@physics.org

dielectric properties of materials nowadays is needed in a wide range of fields, from medical to food sciences, besides electrical engineering and physics. Therefore a deeper understanding of dielectric mixtures is of great value, either for calculating the dielectric constant of a mixture of substances with known dielectric constants or, knowing the dielectric constant of a mixture of two components and that of one of the components, for deducing the dielectric constant of the other component [1–6]. It would also be useful to be able to estimate the morphology of a mixture of two components, knowing the dielectric constant of the mixture and of the components [4, 5, 7]. Recently, it has been shown that the application of the knowledge in dielectric relaxation phenomena could be used to extract the structure/property relationship in composite dielectrics [4, 5, 8]. The dielectric data of materials are often analyzed with empirical expressions; however, here we shall explicitly show that the unorthodox distribution of relaxation times technique yields significant information about the dielectric properties of composites.

In this paper we investigate the dielectric properties of paraffin wax filled with hollow dielectric–metal–dielectric layered spheres [9]. The employed particles are designed for electromagnetic (radar) absorber applications. Due to the fact that the metal-coated-hollow spheres are lightweight, using them in a particular dielectric matrix would make the composite lighter compared to other metal-filled electromagnetic shielding composite materials. In addition, an extra layer of dielectric is applied to mitigate conduction because of percolating metal layers when high inclusion loads are prepared. Samples with various filler volume fractions, q (nominally $q = 0.1, 0.2, 0.3$ and 0.5), were prepared and their frequency-dependent impedances were measured and characterized on a broad frequency window $0.1\,\mathrm{mHz}$ to $10\,\mathrm{MHz}$ at room temperature. The distribution of relaxation times approach, which yields a relaxation spectrum, is applied to demonstrate its effectiveness. The method aids a comprehensive understanding of individual relaxations and their origin; we would be able to differentiate where the relaxations are originated. The relaxation spectra of the samples vary as a function of the filler concentration. We also discuss some observed variation in the relaxation time spectra of samples whose filler concentrations are nominally the same.

2. Background

Dielectric properties of materials are expressed as a complex number known as the permittivity ε, whose real ε' and imaginary ε'' parts are proportional to the energy stored and dissipated in the medium, respectively. Although in theory dielectrics are considered to be perfect electrical insulators, when measurements are performed it is usually non-trivial to separate the conduction and polarization from each other at low frequencies ν, where ohmic losses influence the measurements [10–13]. Therefore, any immittance level representation (permittivity ε^*, modulus $\mathrm{M}[\equiv (\varepsilon^*)^{-1}]$, conductivity $\sigma^*(\equiv \iota\varepsilon_v\varepsilon^*\omega)$ and resistivity $\rho^*[\equiv (\sigma^*)^{-1}])$ of a measurement, yields the same information related to the material properties. Here, $\varepsilon_v = 8.854\,\mathrm{pF\,m^{-1}}$ is the permittivity of free space (vacuum), $\omega = 2\pi\nu$ and $\iota \equiv \sqrt{-1}$.

Noting this we can in general express the complex dielectric permittivity ε^* of a material as follows,

$$\varepsilon^* = \varepsilon' - \iota\varepsilon''$$
$$= \varepsilon_\infty + \chi^* + \sigma_0(\iota\varepsilon_v\omega)^{-1}. \tag{1}$$

In equation (1), instantaneous polarizations in the material are summed in the high-frequency dielectric permittivity value denoted by ε_∞. Dispersions due to conductive or dielectric relaxations are included in the complex dielectric susceptibility χ^*, which has real and imaginary parts χ' and χ'', respectively. The conduction (ohmic) losses from the direct current conductivity σ_0 are included in the imaginary part of the complex permittivity ε''. Consequently the two material constants ε_∞ and σ_0 and the frequency-dependent susceptibility can be employed to describe the electrical/dielectric characteristics of a material. As a note, the listed material parameters above are functions of state variables, such as temperature, frequency, electric field, pressure, etc.

As mentioned before, one of the immittance levels would be appropriate for analysis of the broadband impedance spectroscopy data. We adopt the frequency-dependent complex dielectric permittivity $\varepsilon^*(\omega)$ and complex resistivity $\rho^*(\omega)$:

$$\rho^*(\omega) = [\iota\varepsilon_v\varepsilon^*(\omega)\omega]^{-1}. \tag{2}$$

The complex resistivity representation is more appropriate for conductive systems [11–14]. At low frequencies the ohmic conductivity σ_0 of the samples influences the imaginary part of the permittivity, which hinders the visibility of plausible relaxation processes. Throughout the text we present our data in this representation because of its advantage in observing the ohmic losses easily. In addition, in dispersive systems, sometimes the dielectric losses due to polarization effects and non-ohmic charge transfer mechanisms are misinterpreted as pure ohmic losses.

In the distribution of relaxation times formalism, the complex dielectric susceptibility $\chi^*(\omega)$ in equation (1) is expressed as [15–24],

$$\chi^*(\omega) = \int_{-\infty}^{\infty} g(\tau)(1 + \iota\tau\omega)^{-1} d\log_{10}(\tau) \tag{3}$$

where τ is the relaxation time. The distribution function $g(\tau)$ bears valuable information about the material in hand. (Different notations for the distribution function have been used; see [17, 23] and reference therein. In this study we denote it with $g(\tau)$, which is the distribution of relaxation times in the base 10 logarithmic scale; the inverse problem at hand is treated in the logarithmic scale.) It can be related to the structure of the composite [4, 5, 7, 8, 14] and molecular relaxations [17–19, 25–27]. We adopt a numerical method developed to extract the distribution function $g(\tau)$, based on the Monte Carlo technique and Bayesian statistics. The numerical procedure is explained explicitly elsewhere [7, 14, 20, 28].

Although we have applied a couple of mixture expressions to estimate the frequency-dependent permittivity of the beads from the measured impedances,

the obtained results were not sufficiently good to pursue application of the spectral density representation method for the structure/property relationship analysis of this system [5, 7, 29]. For this reason, the distribution of relaxation times approach is employed [20–23]; note the analogy between the distribution of relaxation times and the spectral density representation approaches [8]. Besides the frequency-dependent properties, the high-frequency dielectric permittivity values of the samples can be described with the Lichtenecker mixture expression [30].

3. Materials and methods

The filler particles were formed by sputter deposition of tungsten onto hollow glass microspheres (3M Scotchlite[TM]S60 glass microbubbles) [31]. An additional coating of alumina prevents oxidation of the tungsten and insulates against the formation of conducting pathways in the composite. This has the benefit that the interfacial polarization process can be studied in isolation from conduction effects. The core particle mean radius is 15 μm, but there is significant variation about this mean.

Mixtures were prepared for filler volume fractions in the nominal range 0–0.5 by hand blending pre-weighed quantities of the filler and matrix on a hot plate at a temperature above the melting point of paraffin wax (approximately 60°C). Once the wax had melted the mixture was removed from the heat and mixing continued until solidification occurred. Samples were then formed by cold-pressing cylindrical disks with diameter 10 mm. Electrodes on either side of the sample were formed by the application of silver-loaded conductive paint. Impedances of the samples were measured with a Novocontrol Alpha Dielectric Spectrometer between 0.1 mHz and 10 MHz. The experimental measurements were first presented in reference [9], in which further details can be found.

4. Results and discussion

The complex resistivity ρ^* of the samples as measured are shown in figure 1. In the inset of figure 1, the real part of the complex conductivity σ^* is presented as a function of frequency. First we observe that the samples do not indicate any obvious ohmic conductivity σ_0, which would be clearly seen in these graphs as straight lines; the Argand plot of the complex resistivity should yield a constant $\log \rho'$ for $\log \rho'' \to -\infty$, which would be located at the lower right corner in the figure, or $\lim_{\omega \to 0} \sigma'(\omega) = \sigma_0$, which is the far left-hand side of the inset. Observe that the resistivity increases as the angular frequency decreases, cf. figure 1. Although $\sigma'(\omega)$ of some of the samples appear to be constant in the inset, the dielectric dispersion is broad as if it is a constant-phase-angle, or low-frequency-dispersion type of relaxation in these samples [10, 13, 32], which is clear in the Argand plot. The dielectric response of the samples indicate a sum of polarization and the constant-phase-angle processes, cf. figure 2. The constant-phase-angle sort of relaxation behaviour is constantly recorded in densely filled composites and systems with hopping conductivity [10, 13]. Finally the samples with the highest bead concentration show a tendency for ohmic losses at low
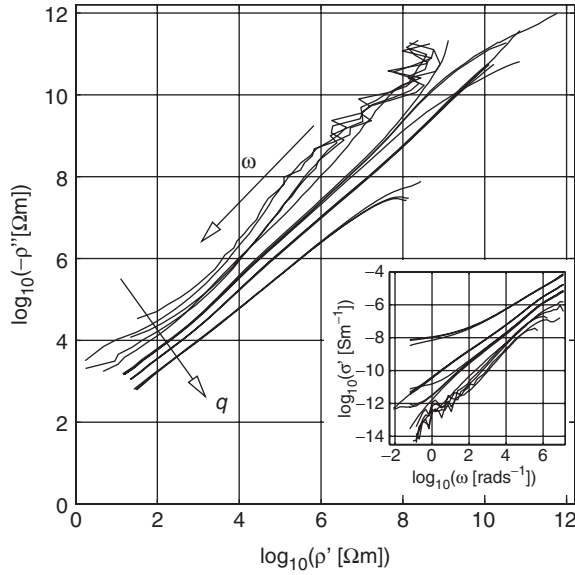
Figure 1. Argand plot of the complex resistivity ρ of the composites studied here. The arrows indicate the increasing angular frequency ω and bead concentration q. The inset shows the real part of the complex conductivity σ as a function of angular frequency ω.

frequencies because the complex resistivity plots indicate a knee point around $\log \rho' \sim 8$ and $\log \rho'' \sim 7.8$.

In figure 2, the complex susceptibility of the sample with $q = 0.20$ is shown as an illustration for the distribution or relaxation times approach presented here. The numerical procedure (the solid lines) reconstructs the original data (presented with open symbols) with good quality. The resolved distribution of relaxation times for this particular sample is shown as an inset in the figure. Observe that there are two visible peaks, one at long times $\tau \sim 100\,\text{s}$ and one at short times $\tau \approx 1\,\mu\text{s}$. The response in between is very broad, spanning several decades. The two visible peaks can also be observed in the complex susceptibility χ^* but not as clearly as in the relaxation spectra in the inset. If only the losses χ'' are taken into consideration, the response at low frequency ($\omega < 10\,\text{rad s}^{-1}$) can easily be mistaken for an ohmic loss, $\chi'' \equiv \sigma_0(\varepsilon_0\omega)^{-1}$. However, χ' increases with decreasing angular frequency and the ohmic conductivity contribution is not obvious. The numerical procedure applied here, on the other hand, uses both the real and the imaginary parts of the immittance data. The solutions therefore satisfy the Kramers–Kronig relations [33] and the actual conductivity can be estimated. The conductivities of the samples therefore are estimated in each Monte Carlo step; see [20] for details.

Now that the validity of the applied numerical procedure has been shown, we can resolve the distribution of relaxation times spectra for all of the samples in hand. In figure 3, the estimated distributions are plotted as both three-dimensional and two-dimensional graphs. In figure 3a, the relaxation spectra are shown as functions of concentration q and relaxation time τ. In figure 3b, the filler
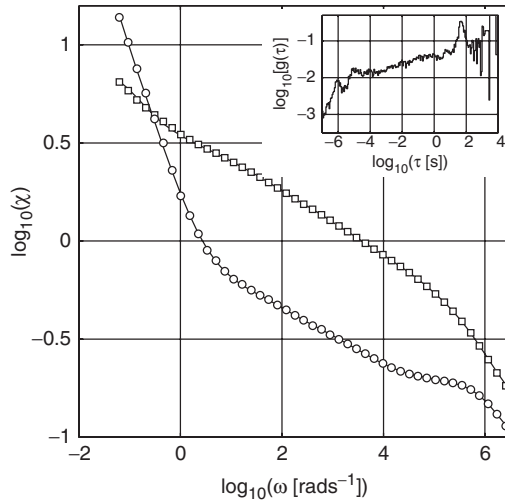
Figure 2. The real and imaginary parts of the complex dielectric susceptibility χ^* as a function of angular frequency ω for $q = 0.20$. The real (χ'; $\square$) and imaginary ($-\chi''$; $\bigcirc$) parts are shown with open symbols. The solid lines (—) are calculated with the estimated resolved distribution of relaxation times $g(\tau)$, equation (3), shown in the inset.
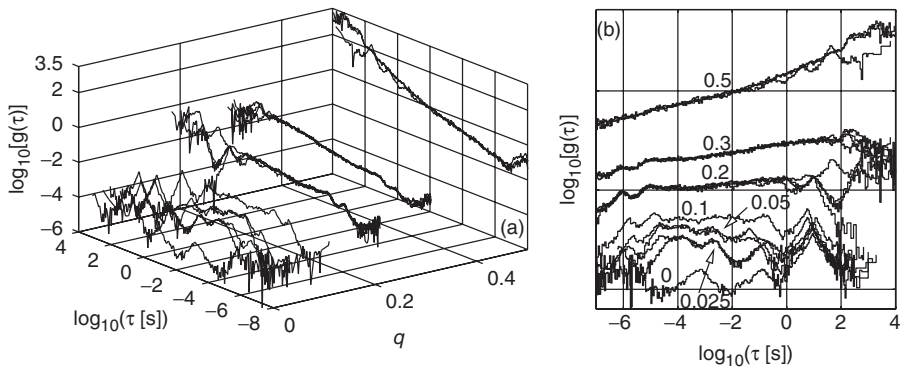

Figure 3. The distribution of relaxation times spectra; (a) three-dimensional graphical illustration and (b) the same data as in (a) but shifted and presented in arbitrary units. The concentration q of beads is shown on each curve in (b).

concentrations q for the obtained distributions are marked for each curve. The evolution of the distribution of relaxation times as a function of filler volume fraction is obvious, and two points are worthy of mention:

(i) The relaxation spectra for intermediate times $(1 \, \mu s \lesssim \tau \lesssim 1 \, s)$ have the highest variation with increasing bead concentration q when $q < 0.2$. Note that there is a new broad relaxation at $100 \, \mu s$ with the introduction of the filler particles into the paraffin wax which, alone, does not exhibit a relaxation at around this time scale.

(ii) As the concentration of the filler is increased, with $q > 0.1$, visible peaks in the spectra diminish and a clear, very broad distribution emerges.

It is striking that the distributions obtained for various samples with nominally the same filler volume fraction indicate very similar spectra at short times ($\tau \lesssim 100\,\mathrm{ms}$) whereas, at long times ($\tau \gtrsim 100\,\mathrm{ms}$), there are slight differences which provide clear evidence of structural deviations between the samples, e.g. the distribution of the filler particles. If the disorder inside the samples and the conduction and polarization process are taken into consideration, the slight deviations could be related to or be perceived as the hopping conductivity contribution and the hopping sites that the charge carriers can access. Samples with a smooth, broad distribution spectrum have a continuous chain of sites for the charge carries to hop without any disruption. However, if there are peaks in the spectrum that can be realized to be an indication of a distribution or more likely an interaction of carriers with the local environment. It can also be related to the interfacial polarization and size distribution of fillers [32], which influence the local electric field, and therefore the internal polarization of a sample. Due to the differences between the conductivities and permittivities of adjacent phases, the charge carriers relax with different rates. The pure wax does not indicate any significant dielectric loss due to the ohmic conductivity. Therefore, although we have not deeply investigated what the mobile hopping charge carriers might be, the hopping charge carrier species might originate from the alimuna dielectric layer or the presence of the trapped ambient humidity during the preparation of the samples.

Although the arguments presented may sound speculative, to our knowledge there are no other statistical studies on the dielectric properties of these kinds of composites. The reason for this is that, often, investigations on and results for a single sample are reported, and deviations between individual (but nominally similar) samples are not considered. To clarify this point, we show the relaxation spectra of three individual samples with $q = 0.20$ filler content in figure 4. Observe the difference in the spectra for $\tau > 1\,\mathrm{s}$. The internal bead distribution influences the low-frequency dielectric properties of the composite. Numerical investigation on disordered binary mixtures have also yielded similar results [32, 34, 35].

To illustrate the way in which the relaxation spectrum of the paraffin wax changes on introduction of the filler, spectra of the unfilled matrix and dilute mixtures are shown in figure 5. The relaxation peaks resolved for the matrix alone ($q = 0$) are marked with '*a*', '*b*' and '*c*' for short times to long times in the figure. The numerical method extracts the dielectric relaxation at long times, peak *c*, clearly, $\tau \approx 10\,\mathrm{s}$ for dilute samples. Since this peak is visible in all the estimated spectra presented in the figure, with only a slight shift in position as filler is introduced, this relaxation is supposed due purely to the paraffin wax. The relaxation at $\tau \approx 0.1\,\mathrm{s}$, peak *b*, is on the other hand enhanced with the inclusion of the filler. This behaviour might be explained by the change of the local field and its contribution to the amplitude of the dipolar relaxation in the paraffin wax, as filler is introduced. For this particular relaxation for the samples with $q = 0.05$ and for the relaxation at $\tau \approx 1\,\mathrm{ms}$, peak *a*, there is a slight shift in the position of the relaxation as filler is added but the enhancement is still visible. Similar behaviour was previously observed in low-density polyethylene filled with a small amount of titanium dioxide composite [36], which again used impedance spectroscopy as a probing technique. The relaxation at $\tau \approx 1\,\mathrm{ms}$, peak *a*, becomes broader with increasing bead concentration, indicating that this relaxation contains an
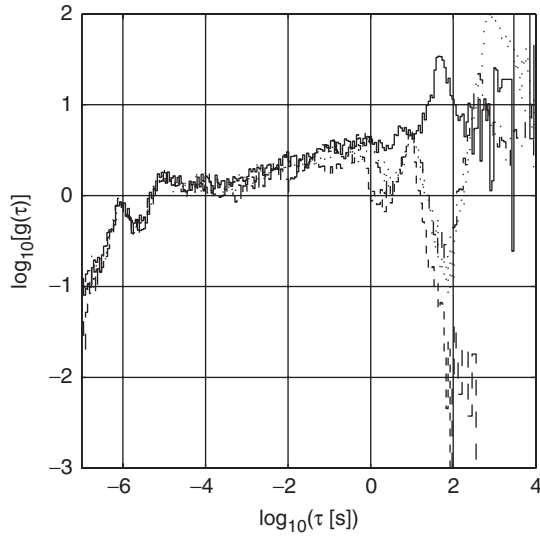
Figure 4.   The distribution of relaxation times spectra for three composite samples with $q = 0.20$.
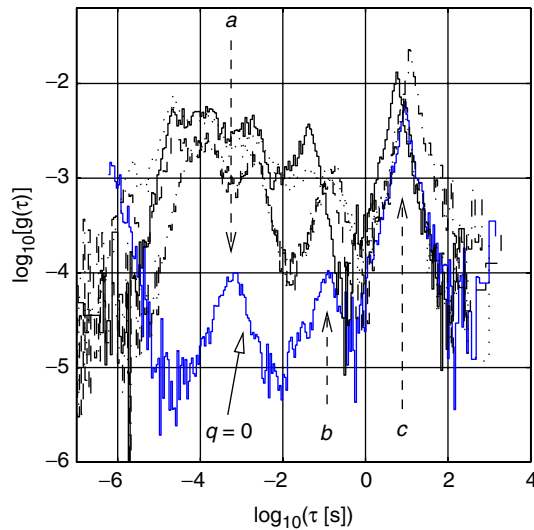

Figure 5.   The distribution of relaxation times spectra for the composites with $q < 0.1$. The solid (—) and dotted (······) lines represent the spectra for the samples with $q = 0.05$. The dashed (- - -) and chain (—·—) lines represent the spectra for the samples with $q = 0.025$. The relaxations instinct to the matrix are labelled with '*a*', '*b*' and '*c*'.

actual contribution from the filler bead particles. In Raman spectroscopy, spherical metal particles are used to enhance the electrical field and improve the signal quality for better probing of material properties [37]. The enhancement of the relaxation peaks observed here as filler is introduced appears to be a similar phenomenon.
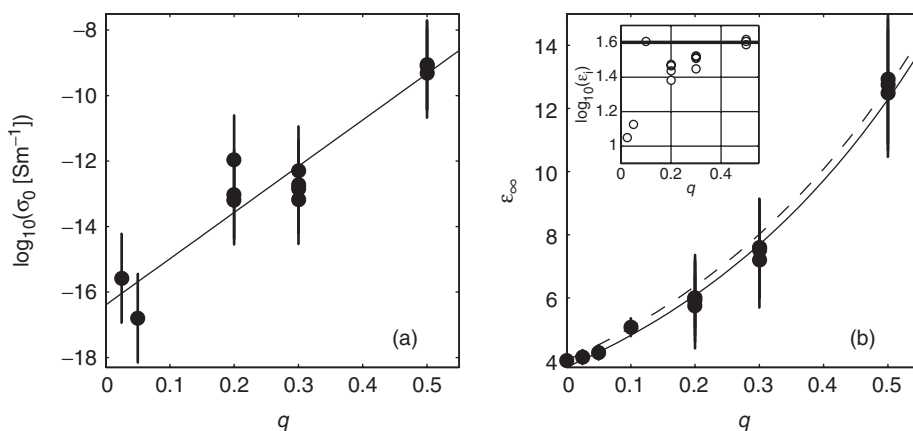
Figure 6. (a) The ohmic conductivity σ_0 and (b) the permittivity ε_∞ of the composite samples as a function of bead concentration q. The solid line (—) in (a) is an exponential fit $\sigma_0 = B\exp(Aq)$ with $B = 4.03 \times 10^{-17}$ and $A = 32.5$. The solid line (—) in (b) is an exponential fit $\varepsilon_\infty = b\exp(aq)$ with $b = 3.80$ and $a = 2.34$. The inset in (b) illustrates the permittivity of the inclusion beads calculated from the Lichtenecker [30] expression; the solid horizontal line in the inset denotes the high-frequency permittivity of the inclusions, $\varepsilon_{i\infty}$. The dashed line (- - -) in (b) is the Lichtenecker [30] expression calculated with the high-frequency permittivity of the matrix $\varepsilon_{m\infty} = 4$ and $\varepsilon_{i\infty} = 40$.

The material constants, ohmic conductivity σ_0 and estimated instantaneous dielectric permittivity ε_∞ are shown as a function of bead concentration in figure 6. The ohmic conductivities of the samples increase with increasing bead content, figure 6a. However, the values show some scatter, which is presumed due to the topological differences between the samples. The error bars are due to the statistical analysis of the result obtained from the Monte Carlo procedure. For clear ohmic losses the error bars are negligible, see [20]. The instantaneous permittivity $\varepsilon_\infty[\equiv \varepsilon(\omega > 1\,\mathrm{MHz})]$ of the samples exhibits a clearer dependence on the filler fraction. Even the deviation in the permittivity values between individual samples with the same nominal filler fraction is smaller than seen in the values of σ_0. The permittivity data can successfully be fitted with an exponential relation. Extrapolation of the fitted curve in figure 6b yields a high-frequency dielectric permittivity value for the beads, $\varepsilon_{i\infty} \approx 40$. The data can also be well-approximated by the Lichtenecker [30] expression with the high-frequency permittivity of the matrix $\varepsilon_{m\infty} = 4$ and $\varepsilon_{i\infty} = 40$, also shown in figure 6b.

5. Conclusions

In this letter we have shown that the dielectric properties of composites can be investigated with the distribution of relaxation times approach. The results have indicated that the dielectric relaxations intrinsic to the matrix can be separated from the relaxation spectra of the filled composite. In addition, differences between the relaxation spectra of nominally similar samples can also be observed and investigated. In the future, this kind of observation could be used to tailor the

design of the material. The high-frequency, $\varepsilon(\omega > 1\,\mathrm{MHz})$, dielectric permittivity value for the filler particles obtained via the distribution of relaxation times approach was shown to be well-approximated by the Lichtenecker mixture formula.

In order to design better composite materials for electrical applications, it is obligatory to better understand the polarization and conduction mechanisms in composites. The utilized non-parametric dielectric data analysis method has an advantage over other parametric methods, which are based on *a priori* assumptions, such as the number of relaxations, type of relaxation model, initial guess, etc. As shown explicitly here, this non-parametric method does not suffer from these drawbacks.

Acknowledgment

References

[1] H.H. Lowry, J. Franklin Inst. **203** 413 (1927).
[2] A. Sihvola, *Electromagnetic Mixing Formulas and Applications*, IEE Electromagnetic Waves Series, Vol. 47 (The Institute of Electrical Engineers, London, 1999).
[3] D.J. Bergman and D. Stroud, Solid State Phys. **46** 147 (1992).
[4] E. Tuncer, Phil. Mag. Lett. (6) 269 (2005); preprint cond-mat/0503710.
[5] E. Tuncer, J. Phys. D: Appl. Phys. **38** 223 (2005); preprint cond-mat/0403468.
[6] E. Tuncer, Y.V. Serdyuk and S.M. Gubanski, IEEE Trans. Dielect. Elect. Insul. **9**(5), 809 (2002); preprint cond-mat/0111254.
[7] E. Tuncer, Phys. Rev. B **71** 012101 (2005); preprint cond-mat/0403243.
[8] E. Tuncer, J. Phys.: Condens. Matter **17**(12) L125 (2005); preprint cond-mat/0502580.
[9] N. Bowler, I.J. Youngs, K.P. Lymer and S. Hussain, in *2004 Annual Report* (IEEE Dielectrics and Electrical Insulation Society, 2004), Conference on Electrical Insulation and Dielectric Phenomena (CEIDP), Vol. I, pp. 381–384.
[10] A.K. Jonscher, *Dielectric Relaxation in Solids* (Chelsea Dielectric, London, 1983).
[11] J.R. Macdonald, Brazil. J. Phys. **29**(2) 332 (1999).
[12] J.R. Macdonald, J. Non-Cryst. Solids **212** 95 (1997).
[13] J.R. Macdonald (Editor), *Impedance Spectroscopy* (John Wiley, New York, 1987).
[14] E. Tuncer, *The Landau-Lifshitz/Looyenga Dielectric Mixture Expression and its Self-Similar Fractal Nature*, Unpublished (2005); preprint cond-mat/0503750.
[15] H. Fröhlich, *Theory of Dielectrics; Dielectric Constant and Dielectric Loss*, 2nd ed. (Oxford Science Publications, Oxford, 1958).
[16] B.K.P. Scaife, *Principles of Dielectrics* (Oxford Science Publications, Oxford, 1998).
[17] C.J.F. Böttcher and P. Bordewijk, *Theory of Electric Polarization*, 2nd ed. Chap. IX, (Elsevier, Amsterdam, 1996), pp. 45–137.
[18] N.G. McCrum, B.E. Read, and G. Williams, *Anelastic and Dielectric Effects in Polymeric Solids*, Dover ed. (John Wiley, London, 1967).
[19] E. Tuncer, M. Furlani, and B.E. Mellander, J. Appl. Phys. **95**(6) 3131 (2004).

[20] E. Tuncer and S.M. Gubański, IEEE Trans. Dielect. Elect. Insul. **8** 310 (2001).

[21] E. Tuncer and J.R. Macdonald, *Comparison of Methods for Estimating Continuous Distributions of Relaxation Times*, Unpublished (2004); preprint cond-mat/0504428.

[22] J.R. Macdonald, J. Comp. Phys. **157** 280 (2000).

[23] J.R. Macdonald, Inv. Problems **16** 1561 (2000).

[24] R.L. Wolpert, K. Ickstadt and M.B. Hansen, in *Bayesian Statistics 7*, edited by M.J. Bernardo, M.J. Bayarri, J.O. Berger, *et al.* (Oxford University Press, Oxford, 2003), pp. 403–418.

[25] A. Bella, E. Laredo, and M. Grimau, Phys. Rev. B **60**(18), 12764 (1999).

[26] M. Grimau, E. Laredo, A. Bello, *et al.*, J. Polymer Sci. B: Polymer Phys. **35** 2483 (1997).

[27] E. Tuncer, M. Wegener and R. Gerhard-Multhaupt, J. Non-Cryst. Solids **351**(33-36) 2917 (2005).

[28] E. Tuncer and S.B. Lang, Appl. Phys. Lett. **86** 071107 (2005); preprint cond-mat/0409183.

[29] D.J. Bergman, Phys. Rep. **43**(9) 377 (1978).

[30] K. Lichtenecker, Z. Phys. **27** 115 (1926).

[31] C.S. Chamberlain, G. Connell, and W.C. Tait, *Electromagnetic Radiation Absorbing Material Employing Doubly Layered Particles*, US Patent, 5,389,434 (1995).

[32] E. Tuncer, J. Phys. D: Appl. Phys. **37** 334 (2004); preprint cond-mat/0403244.

[33] L. Landau and E. Lifshitz, *Electrodynamics of Continuous Media*, 2nd ed. Vol. 8 Course of Theoretical Physics, (Perganom Press, New York, 1982).

[34] E. Tuncer, S.M. Gubański and B. Nettelblad, J. Appl. Phys. **92**(8) 4612 (2002).

[35] J.P. Calame, J. Appl. Phys. **94**(9) 5945 (2003).

[36] P. Frübing, D. Blischke, R. Gerhard-Multhaupt and M.S. Khalil, J. Phys. D: Appl. Phys. **34**(20) 3051 (2001).

[37] H.P. Lu, J. Phys.: Condens. Matt. **17**(7) R333 (2005); http://stacks.iop.org/0953-9984/17/R333